IMPACT TEST ANALYSIS OF ALUMINUM ALLOY WHEELS UNDER DIFFERENT TEMPERATURE

Ümit Elmahti and Paşa Yayla
Mechanical Engineering Department, Marmara University Engineering Faculty, Istanbul, Turkey

Ahmet Yiğit Kaya and Onur Özaydın
R & D Department, Cevher Jant Sanayii A.Ş., İzmir, Turkey

https://doi.org/10.1007/s40962-022-00845-2

Abstract

Aluminum alloy wheels are used worldwide in both the warmest and coldest temperatures. This study was conducted to investigate the impact resistance of aluminum alloy wheels produced by the low-pressure die casting process in real-life conditions. The V-notched Charpy impact test specimens were extracted from T6 heat-treated A356 aluminum alloy wheels. These specimens were tested with an instrumented Charpy V-notched impact tester after being conditioned at temperatures of − 75, − 40, 0, 20, 60, 95, and 175 °C. Charpy impact test diagrams of load-time and energy-time were created. The average crack initiation Charpy impact strength, average crack propagation Charpy impact strength, and average total Charpy impact strength values at different temperatures were calculated. Analysis of the fracture surfaces was performed using a scanning electron microscope (SEM), and the microstructure was analyzed using optical microscopy. In addition, the chemical characterization of the samples was performed by energy-dispersive spectroscopy (EDS) and optical emission spectroscopy (OES). The results of all the instrumented Charpy impact tests, together with the macroscopic and microscopic fracture surface examinations, revealed important results on the nature of fracture and the effects of different temperatures. The study revealed the variations of the Charpy crack initiation, crack propagation and total impact strengths as a function over a wide range of temperatures.

Keywords: *aluminum alloys, instrumented Charpy impact strength, temperature effects, micro- and macrostructure*

Introduction

Aluminum is one of the most extensively preferred light metals owing to its castability ease as well as good corrosion properties, and sufficient specific strength. These properties of aluminum ensure its wide use in automotive industry products such as wheels.[1,2] Wheels are used in various temperatures, from the coldest areas to deserts. The maximum operating temperature of the wheels can reach about 150 °C.[3] Therefore, the aluminum alloy used to produce wheels should be selected considering its behavior in these extreme temperature conditions. Nowadays, many wheels are made of A356 alloy by the low-pressure die casting (LPDC) process.[1,4] A356 hardens by precipitation. Therefore, the impact strength, which is critical for wheels, can be increased by heat treatments.[5–8] For example, a homogenization heat treatment phase at 540 °C in less than 6 hours results in an optimum impact strength value. Moreover, the impact strength drops significantly after 16 hours of aging.[9] However, Alexopoulos and Stylianos observed that the impact strength also decreases considerably due to over-aging.[10]

Impact fracture is generally unexpected and is influenced by many known factors. Not only is heat treatment a critical parameter, but also the amount of Sr, Fe, Mg, grain size, and microstructure are some of the key factors for fracture toughness.[11–16] Samuel and his co-workers identified a reduction in notched impact strength due to Sr-B interactions in some cases because of microstructural studies. The morphology of the inter-dendritic phases also affects the impact

Received: 25 March 2022 / Accepted: 22 June 2022 /
Published online: 18 July 2022

toughness. The best toughness value was observed in Al5TiB grain refinement samples with 200 ppm Sr addition in T6 heat treatment compared to the addition of 30 ppm Sr and Al10Ti master alloy.[17] Tillová et al. also investigated whether Sr addition in an AlSi11Mg alloy positively affected impact strength. 0.05, 0.1, and 0.15% Sr were added to the samples. The best fracture toughness was observed in the sample with a 0.05% Sr addition.[18] Amne Elahi et al. (2016) concluded that the grain refinement and modification separately caused an increase in impact strength. Moreover, grain refinement did not result in such a large increase in impact strength compared to modification in the as-cast condition (without heat treatment).[5] On the other hand, it should not be forgotten that even if all factors are optimal, pores around the notch can influence the result of notched bar impact testing.[19]

In addition to all these parameters affecting fracture toughness, the effect of operating temperatures is currently being studied, as in the past.[11] According to Lalpoor et al., all specimens tested at temperatures below 200 °C showed relatively fragile properties. At 400 °C, they showed more ductile behavior. Brittleness was observed with decreasing temperature.[20] It is generally believed that the impact strength increases slightly with temperature for metals with face-centered cubic (FCC) lattice structured metals (e.g., aluminum). However, this increase does not correspond to the ductile, brittle transition temperature observed in the body-centered cubic lattice structure like steel or cast iron. This contradictory behavior is related to the nature of the dislocation motion in the individual crystal lattices.[21,22]

In this paper, an aluminum alloy wheel was cast from an aluminum alloy using a low-pressure die casting process. This aluminum alloy, designated A356, contains a 7% Si and a 0.3% Mg and has undergone T6 heat treatment processes. At the end of the manufacturing process, the aluminum alloy wheels were tested and evaluated to determine mechanical behavior such as fracture and notched impact strength. Some of these tests and investigations are the Charpy V-notch test and macro and microfracture surface inspections.

Experimental Procedure

Sample Production

Melting the ingots in a melting furnace is the first step in the metal preparation process. Degassing is done with nitrogen (N), a liquid metal obtained from the melting furnace. Depending on the metal concentration, different degassing programs are employed in the degassing process. Reference performance tests (RPT) are used to keep the gas level under control. Sr is added as a modifier, and TiBor is added as a grain refiner.

The wheels are produced by low-pressure die casting, and the material of these wheels is A356 aluminum alloy, which is a hypoeutectic aluminum alloy. Table 1 contains the results of the chemical composition analysis of the alloy as measured with an optical emission spectrometer.

The ingots were first melted at 750 ± 5 °C. These wheels were cast from the same molten metal to minimize the error caused by chemical composition. Then the wheels are put into the heat treatment phase, which was taken 545 ±5 °C into the solution for 3.5 h, quenched in a water bath at 72 ±5 °C, and then artificially aged at a temperature of 165 ±5 °C for 2 hours. Similar heat treatment conditions were also used for the same material in the literature.[23–28] After heat treatment, the wheels were ready to be machined to produce V-notched specimens.

All wheels were made in accordance with the relevant standards and specifications requested by OEM customers. In this work, the wheels were x-rayed entirely.

The wheels were cast to prepare specimens for the Charpy V-notch impact test. Each wheel has 5 spokes with suitable dimensions for Charpy specimen collection according to TS-EN-ISO 148-3.

Sample Preparation

The Charpy V-notch specimens, extracted from the same product, were cast according to the same chemical composition as mentioned above. Therefore, all test samples are extracted from these spokes, as shown in Figure 1.

In designing the specimens, the utmost care was taken to ensure that the outer flange area was one of the most critical locations for impact resistance.

The standard for the Charpy V-notched bar impact tests is TS EN ISO 148, and according to this standard, the specimens are to have dimensions of 5 mm x 10 mm x 55 mm. First, each wheel was cut from the outer flange and spokes using a band saw for specimen preparation. Then these parts were machined with a milling machine. The most

Table 1. Chemical Composition of A356 Alloy

OES result	Alloying Elements (wt%)								
Sample	Si	Mg	Fe	Mn	Ti	Cu	Sr	Na	Al
A356	7.29	0.28	0.11	0.002	0.12	0.001	0.015	0.0003	Bal.

important part of this machining is the creation of the V-notch. According to the test standard, the V-notch must be 2 mm deep with a radius of 0.25 ±0.025 mm at the root with an angle of 45°±1° to the notch.

Sample Conditioning

The Charpy test method ASTM E23 contains exact requirements for determining and controlling specimen test temperature. It specifies minimum soak times that depend on the use of liquids or gases as the medium for thermal conditioning of the specimen. The method also imposes that the impact of the test sample must be completed within 5 seconds after being removed from the conditioned medium. However, it does not provide any guidance on the choice of conditioning circumference. This study was conducted primarily to investigate the changes in sample temperature when water is used for thermal conditioning. A standard Charpy V aluminum alloy notched bar impact specimen was instrumented with surface-mounted and embedded thermocouples.[29] To test the samples at temperatures between − 75 and 175 °C, acetone and dry ice were used to cool the specimens, and hot water and an electric induction furnace were used to heat the samples.

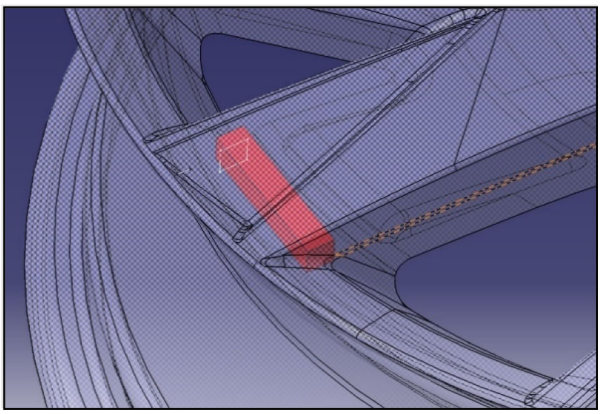

Figure 1. Display of samples taken from the wheel.

Results of Experimental Analysis

Microstructural Analysis

In Figure 2a, shrinkage defects were observed according to the new classification of defects in aluminum alloy casting.[30] These defects may be due to problems related to various reasons. As shown in Figure 2a and b, dendritic α-Al is the most frequently observed structure in the sample's microstructure. As shown in the figure, the Al-Si structure was observed in the sample. It shows that the eutectic Si particles are uniformly distributed in the structure of the Al matrix, as shown in Figure 2. These results are acceptable and fall within stated casting quality limitations; therefore, extracted specimens can be used for Charpy testing.

Six parameters were quantitatively measured on six typical silicon structures corresponding to the AFS chart. The grain size measurements and assessment of modification level is based on the American Foundry Society (AFS) Chart for Microstructure Control in Hypoeutectic Aluminum Silicon Alloys.[31,32]

In Table 2, the microstructural characterization details are noted. First, SDAS values are measured for the specimens pictured in Figure 2. Aguirre-De la Torre et al. measured the SDAS values of A356 wheels after T6 heat treatment and obtained values in the range 40-55 µm.[23] The pictured samples are evaluated as medium-large grain size and non-lamellar-modified modification level.

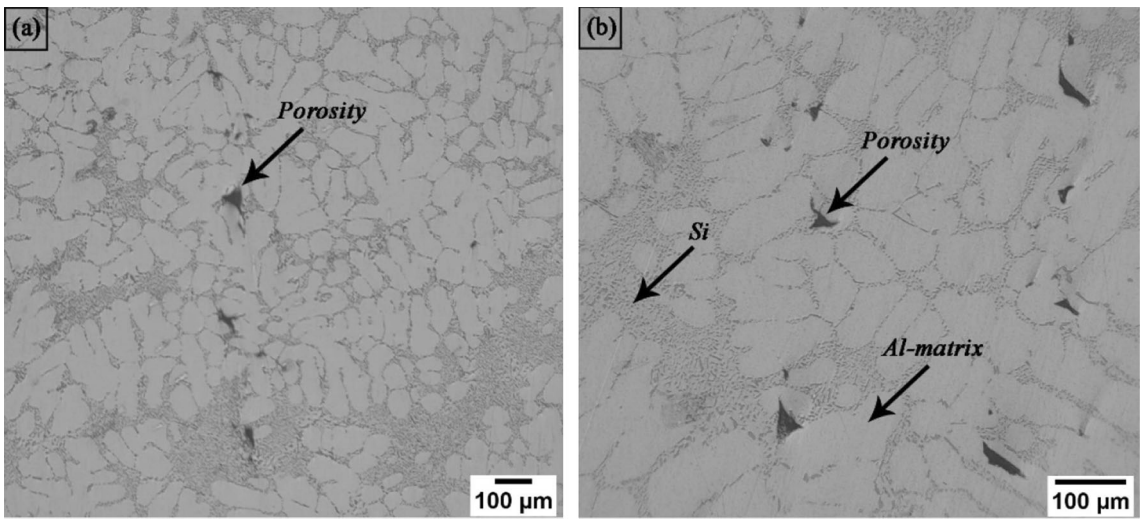

Figure 2. Optic al micrographs of the transverse surface at 50x (a), longitudinal surface at 100x (b).

Table 2. SDAS, Grain Size, % Porosity and Modification Level

		Details
SDAS	Fig. 2a SDAS: 49–50 μm	
	Fig. 2b SDAS: 44–47 μm	
% Porosity	Fig. 2a Porosity 0,08%	
	Fig. 2b Porosity 0,30%	
Grain Size	Proposed Ranking 3–4	3. Medium: Grains per square cm: 217
		4. Large: Grains per square cm: 125
Modification Level (ML)	Type (Class) 4–5	4. Non-Lamellar
		5. Modified

Table 3. Ambient Temperature Tensile Test Results of A356 Aluminum Alloy Wheels Material

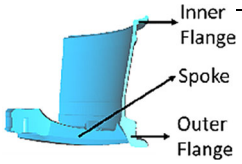

	Regions	Yield strength [MPa]	Ultimate tensile strength [MPa]	Elongation at break (%)
Sample 1	Inner flange	227	291	10.1
	outer flange	220	278	7.3
	spoke	206	258	4.6
Sample 2	Inner flange	227	290	9.6
	outer flange	217	278	9.2
	spoke	207	256	4.7
Sample 3	Inner flange	227	292	8.6
	outer flange	219	281	8.8
	spoke	206	257	5.1

Tensile Test

To determine mechanical properties, tensile tests were performed on certain spoke sections, inner flange, and outer flange. Tensile test specimens were manufactured in accordance with DIN 50125, and each region was tested at least three times using a Zwick Z100 model tensile testing machine in compliance with EN ISO 6892-1, and the results are shown in Table 3.

The tensile behavior of A356 automobile wheel presented in Table 3 is consistent with the findings of Aguirre-De la Torre et al.[23]

Hardness Test

The variation of Brinell hardness distribution in the aluminum wheel is displayed in Figure 3. These measurements were carried out at room temperature on samples in the as-cast and T6 conditioned wheel. As expected, the HB values vary along the wheel section and reach their maximum values around the inner flange.

These Brinell hardness values for T6 heat-treated A356 automotive wheels depicted in Figure 3 are in good agreement with the findings of the Aguirre-De la Torre et al. work.[23]

Impact Strength

The Instron CEAST 9050 impact pendulum impact testing machine was used for this study. The force-time and energy-time response data for 6000 points were obtained with this instrumented Charpy impact testing machine. To obtain the data for 6000 points, the frequency was set to 2000 kHz, and the operating range was set to 100%. The data obtained were converted to graphs using the software of the machine. In addition, OriginPro software was used to create more visually meaningful graphics.

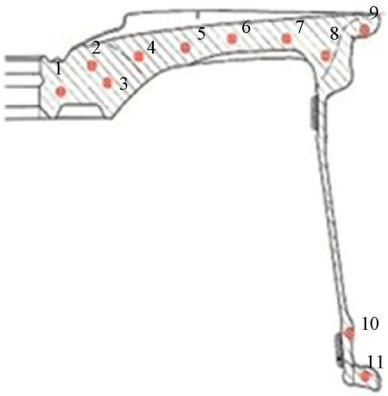

1.	87,4
2.	80,1
3.	83,6
4.	85,0
5.	88,4
6.	87,7
7.	88,3
8.	89,0
9.	89,7
10.	90,6
11.	92,6

Figure 3. Brinell hardness measurements along the wheel section.

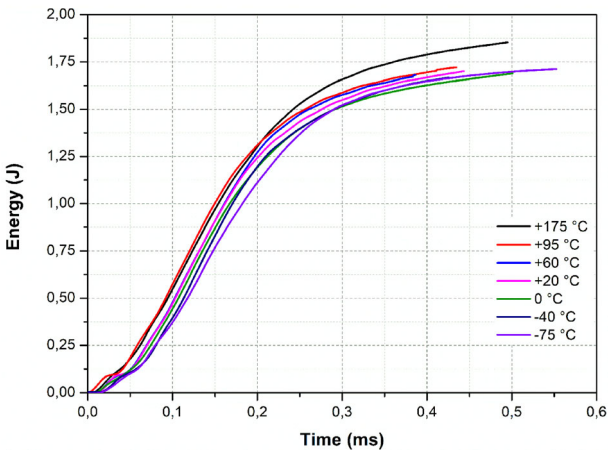

Figure 4. Energy-Time graphs of specimens tested at various temperatures.

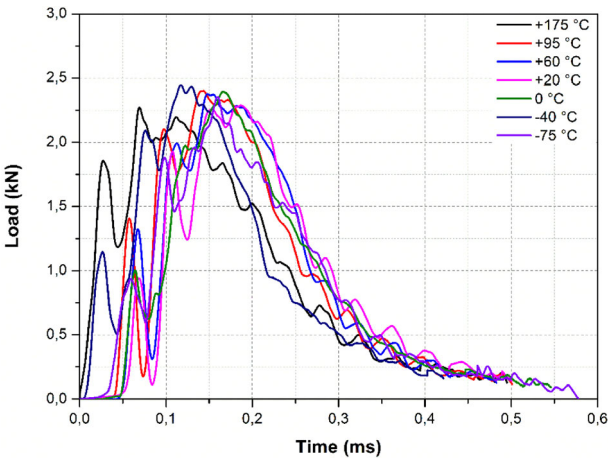

Figure 5. Load-time and graphs of specimens tested at various temperatures.

To estimate the resistance of A356 aluminum wheels produced by the LPDC method at different operating temperatures, the specimens were subjected to impact testing at temperatures of −75, −40, 0, 20, 60, 95, and 175 °C. The crack initiation Charpy impact strength, the

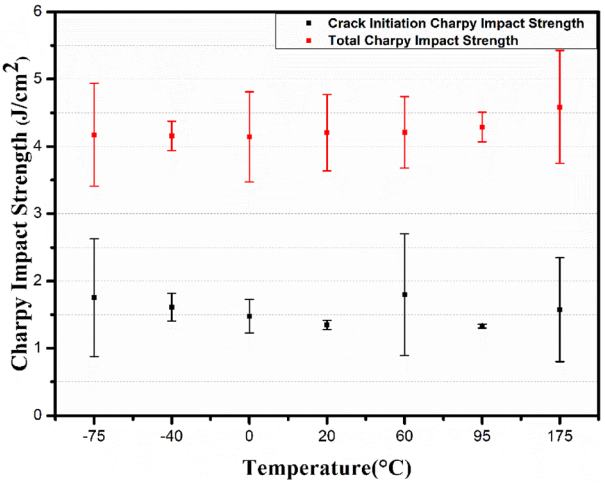

Figure 6. Crack initiation and total Charpy impact strength variation with temperature

Table 4. Load and Charpy Impact Strength Values at Various Temperatures

Temperature [°C]	Average maximum load [kN]	Average crack initiation charpy impact strength [J/cm^2]	Average crack propagation charpy impact strength [J/cm^2]	Average total charpy impact strength [J/cm^2]
175	2.27	1.58	3.01	4.59
95	2.40	1.33	2.96	4.29
60	2.38	1.80	2.42	4.21
20	2.29	1.45	2.75	4.20
0	2.39	1.48	2.67	4.14
− 40	2.44	1.61	2.55	4.16
− 75	2.35	1.75	2.42	4.17

crack propagation Charpy impact strength, and the total Charpy impact strength values were determined from the Charpy impact tests performed at these temperatures. These data were used to investigate the crack resistance of the specimen at different temperatures.

Dry ice, acetone, boiling water, and a vacuum furnace were used to achieve the desired temperature ranges for the specimens. The temperature monitoring was performed during the test using a digital thermometer Greisinger GMH 3201 with a 6010 probe. For thermal insulation of test samples, a system of foam, glass, and polyurethane was used.

The experiments conducted at seven different temperatures, ranging from −75 to 175 °C, are shown in Figures 4, 5, 6 and Table 4. These impact strengths (Table 4 and Figure 6) were determined by dividing the Joule values (Figure 4) from Instron's CEAST 9050 impact pendulum

device by the net cross-sectional area of the sample (0.8 × 0.5 cm). The Load-time and Energy-time diagrams were prepared for each case. In addition, the average maximum load, the average crack initiation Charpy impact strength, the average crack propagation Charpy impact strength, and the average total Charpy impact strength values were also evaluated.

For a wheel made from A356 material, these Charpy impact strength values are in good agreement with the results of the work of Merlin and his co-workers.[19]

Figure 6 shows the average crack initiation Charpy impact strength and total Charpy impact strength values at all temperature conditions. Again, the average crack initiation and total Charpy impact strength variations remain relatively constant along with the test temperatures. However, it is worth pointing out that the average crack initiation Charpy impact strength decreased at test temperatures from 60 to 95 °C, while the average total Charpy impact strength increased slightly.

The results show that the average maximum load of the samples was almost the same for each case. The values varied only between 2.27 and 2.44 kN. Furthermore, the average crack initiation Charpy impact strength decreased from 1.75 J/cm^2 at − 75 °C to 1.45 J/cm^2 at 20 °C. Then there was a sudden slight increase, and the highest value was obtained as 1.79 J/cm^2 at 60 °C. Then, the crack initiation Charpy impact strengths decreased and increased at 95 and 175 °C, respectively. A decreasing trend was observed in the average total Charpy impact strength with a decreasing temperature from 175 to 0 °C. The values below 0 °C, on the other hand, did not change significantly. In addition, the average crack propagation Charpy impact strengths increased with temperature, except for the value obtained at 60 °C. At the maximum test temperature of 175 °C, the highest crack propagation Charpy impact strength of 3.01 J/cm^2 was obtained.

Microstructural Analysis of Fracture Profiles

Fractographic features of the broken Charpy test samples were analyzed by optical microscopy to understand the fracture behavior of the samples tested at different temperatures. A NIKON SMZ 1500 model optical microscope was used to analyze the prepared samples. In the fracture surface image analysis, 20x and 70x magnifications of the optical microscope were used.

In the analyzed fractured surfaces, the highest dimple formation was observed in the samples fractured at 175 °C (Figure 7a). As the test temperature increased, it was observed that there was an increase in the recessed-protruding and fibrous structures on the fracture surfaces of the samples. (Figure 7c). It was also witnessed that the plastic deformation on the fractured surfaces increased with increasing temperature (Figure 7a-c).

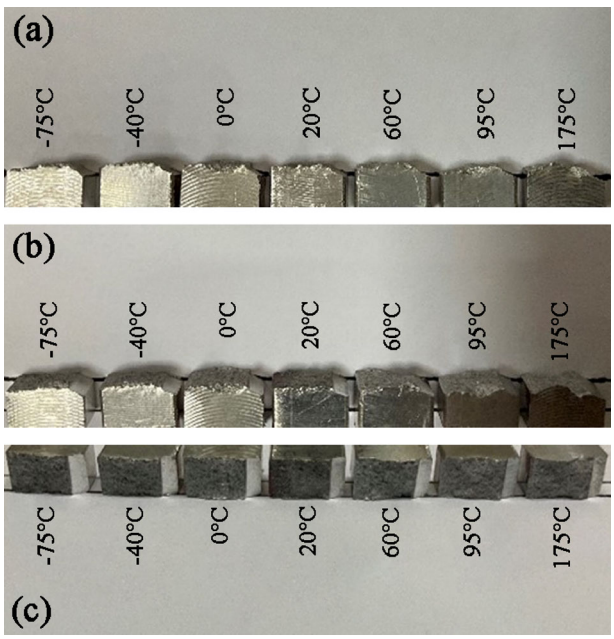

Figure 8. Fractured surface images of a Charpy impact test specimen fractured at different temperatures.

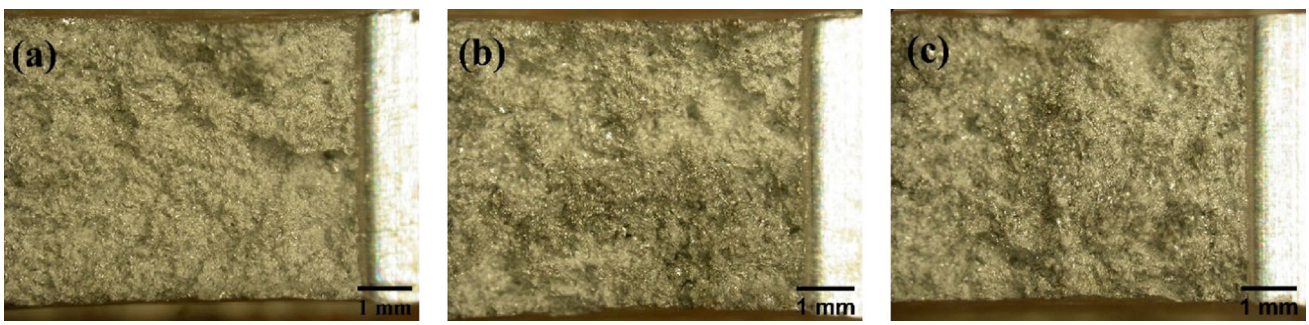

Figure 7. Fracture image of the sample at (a) 175 °C, 20x and (b) at 20 °C, 20x (c) at − 75 °C 20x.

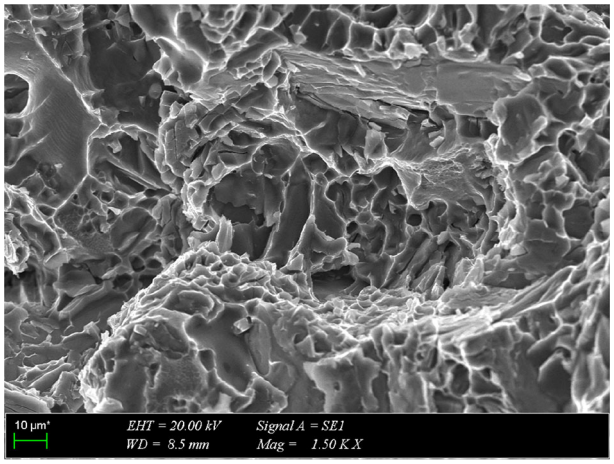

Figure 9. 1500X magnification at 175 °C conditioned sample.

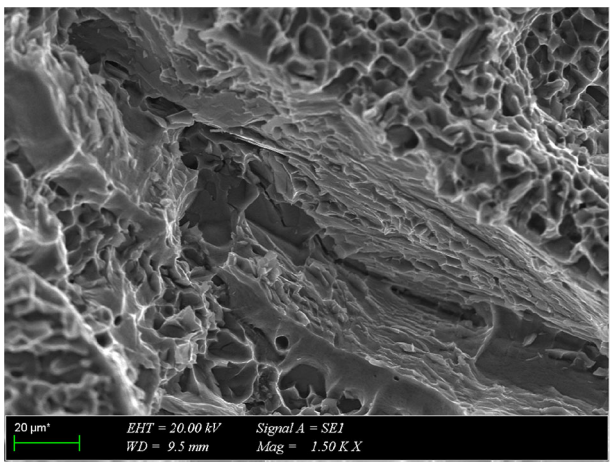

Figure 10. 1500X magnification at 20 °C conditioned sample.

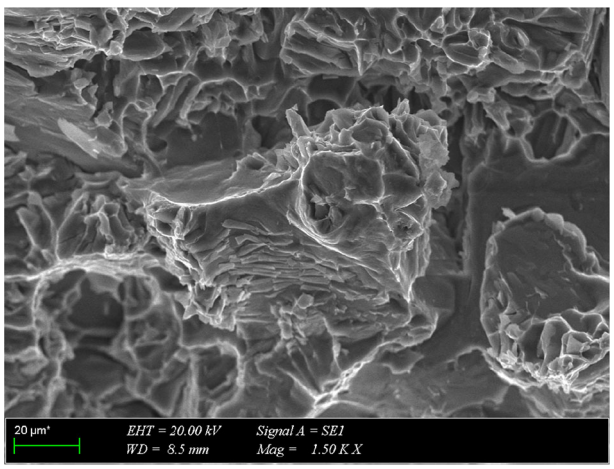

Figure 11. 1500X magnification at − 75 °C conditioned sample.

All photos presented in Figure 8 were taken above and in front of the fractured specimens. The fracture surfaces of samples tested from the coldest test temperature to the highest are presented in Figure 8. The black line was sketched to align the specimens, and it was observed that the fracture became more ductile with increasing test temperature, as expected. Because the fracture line of samples fluctuated with higher test temperatures, the samples tested in colder circumference had a flattered fracture surface.

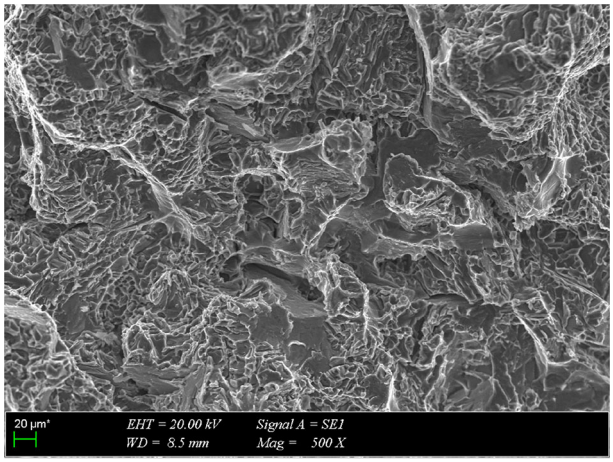

Figure 12. 500X magnification at − 75 °C conditioned sample.

SEM and EDS Analysis of Fracture Surfaces

The in-depth microscopic fractographic analysis of the samples' fracture surfaces at various temperatures was studied with a scanning electron microscope (SEM). In these investigations, ZEISS Evo MA10 is used, and the results are presented in Figs. 9, 10, 11, 12.

At 1500 and 500x magnification, SEM images of the fracture surface were taken from the coldest, room temperature, and warmest conditioned samples. Cleavage and cellular fracture features and transcrystalline fracture of a medium-developed surface were observed in the fracture area of the 175 °C conditioned samples, as shown in Figure 9. Furthermore, cleavage steps developed in the branched particles. The cleavage step system is observed in Figure 11 due to crack front propagation on successive cleavage planes at − 75 °C conditioned sample. Figure 10 depicts a fracture with mixed morphology. In addition, there are oval shear dimples near the cleavage facet.[19,33]

Furthermore, transcrystalline fracture with a highly developed surface and the main crack crossing the silicon precipitate in cleavage planes of various orientations relative to the average fracture plane were observed. Figure 12 depicts the rectilinear secondary cracks, branched cleavage steps, and tear ridges formed in the α-aluminum solution at the 500X magnified sample tested at − 75 °C. At the interfaces of α-aluminum and silicon, well-protected conformation zones can also be seen. Furthermore, the fracture

surface morphology around the deep secondary crack in the sample conditioned at 20 °C was biphasic.[19,33]

The microstructures of the test samples are analyzed using energy-dispersive spectroscopy (EDS), and the results are presented in Figs. 13, 14. EDS was used to examine different visible points of the fractured surface to observe as many different types of microstructures as possible. Figure 13 shows a variety of structures such as secondary cracks, dimples, and micro-necks. The SEM analyses in the vicinity of spot 1 reveal transcrystalline fracture and cleavage facets in the silicon precipitates and brittle intermetallic phases. β-AlFeSi was discovered in Spot 1. The results presented in Figure 14 support the SEM analysis.

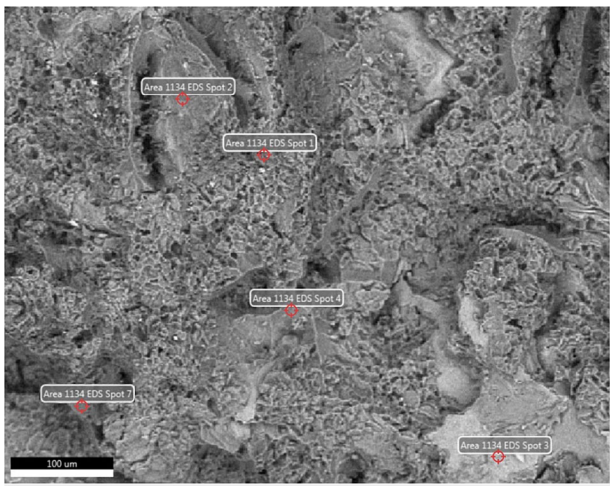

Figure 13. EDS analysis region on the surface of the sample at 20 °C.

Discussion

This study extensively analyzes the instrumented Charpy impact tests carried out on T6 heat-treated A356 aluminum alloy at different temperature conditions. The findings of this study clearly show that as the temperature increased between − 75 and 175 °C, the Charpy impact strength showed a relatively constant pattern. As with other metallic materials with a face-centered cubic crystal (FCC) structure, ductile-brittle transition temperature (DBTT) was not observed within the temperature range studied.

Shivkumar et al.[11] tested V-notched Charpy impact test samples produced from A356 aluminum alloy with different methods at different temperatures from 25 to 200 °C, and they also did not observe a DBTT or significant change in impact energies.

To investigate the DBTT, which cannot be observed in the Charpy impact strength-temperature graph in more detail form, the fracture surfaces of the broken samples in the impact test were examined under optical microscopy and scanning electron microscopy (SEM). This examination may also be valuable to understand the nature of the change in impact energies of the samples tested at different temperatures.

The fracture surface of the samples tested at different temperatures was first examined with the naked eye. In this investigation, it was observed that as the test temperature increased, the plastic deformation on the fracture surface of the samples increased. In addition, on the fractured faces of all samples, characteristic features of ductile fracture such as dull appearance and dimple formation were observed.

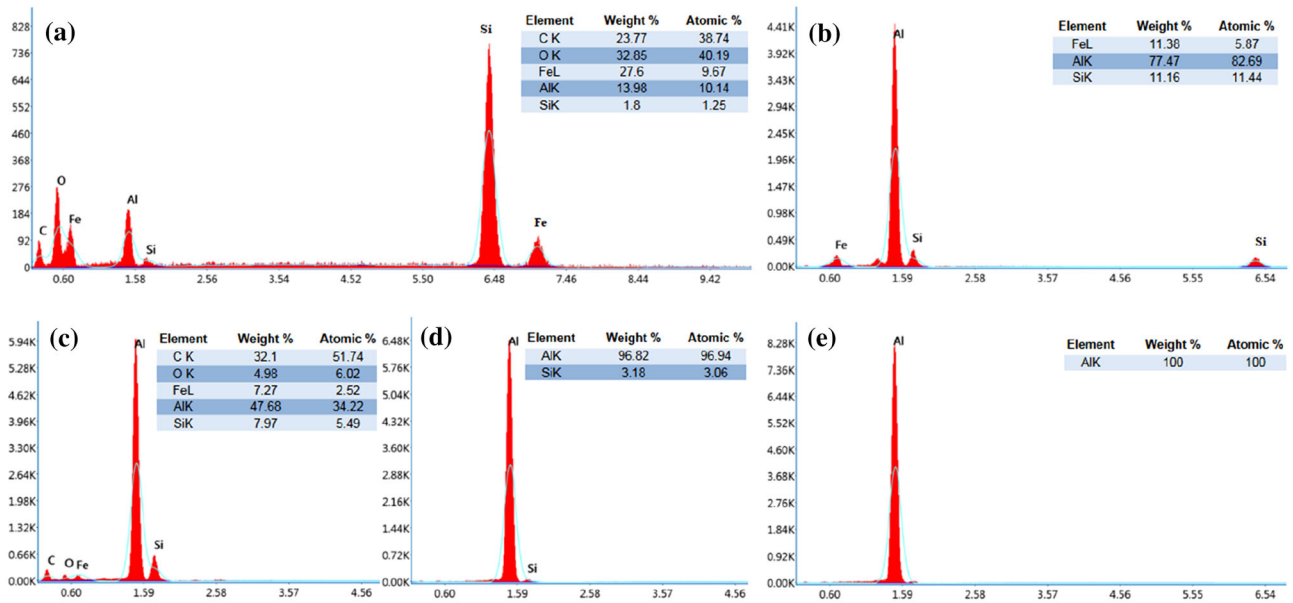

Figure 14. SEM-EDX results of the sample at 20 °C: (a) EDX spot 1, (b) EDX spot 3, (c) EDX spot 2, (d) EDX spot 4, (e) EDZ spot 7.

The SEM analysis was performed to observe the fracture properties of the samples tested at temperatures of − 75, 20, and 175 °C and showed ductile and brittle features. Many fractographic features with brittle and ductile fracture characteristics were observed in this analysis. In general, internal cracks and their accumulation in the dimples were observed at low temperatures. Therefore, it can be interpreted that the samples broken at this temperature show a relatively low impact strength absorption value. It was also found that the size of the dimples increased as the temperature increased. Therefore, as a result of the SEM analysis, it was observed that the general fracture pattern of the A356 Charpy impact test specimens fractured at these temperatures was a ductile fracture in nature.

Conclusions

This research study investigates the effects of a wide range of temperatures on the Charpy impact strength of the wheels produced from A356 aluminum alloy by the LPDC method. The V-notched instrumented Charpy impact tests were carried out to investigate the variations in crack initiation, crack propagation and total Charpy impact strengths over a wide temperatures range of − 75, − 40, 0, 20, 60, 95, and 175 °C. These results are particularly valuable to assess the variations in the toughness of A356 aluminum alloy wheels material taken from real-life conditions.

The V-Notch Charpy impact test results show that the A356 alloy does not have a visible DBTT point. Through the optical examination of the fractured surface, it was observed that as the test temperature increased, the plastic deformation of the fracture surface of the sample also increased.

The SEM analysis of the fracture surface was conducted to reveal additional features and defects. Although the main brittle failure features were detected on the fracture surface of the sample fractured at − 75 °C temperature, more ductile fracture characteristics were detected in the samples tested at high temperatures.

From the instrumented Charpy impact tests and fractographic analysis, it is shown that there is no significant change in the Charpy impact strength of the A356 alloy samples extracted from wheels produced with LPDC at temperatures between − 75 and 175 °C. The instrumented Charpy impact tests at different temperatures revealed that about 36% of the total Charpy impact energy is dissipated due to crack initiation and 64% of the total Charpy impact energy for crack propagation. Based on these findings, it can also be concluded that the temperature range studied in this work does not cause a significant change in the fracture performance of the A356 aluminum wheel material.

REFERENCES

1. D. Sui, Z. Cui, R. Wang, S. Hao, Q. Han, Effect of cooling process on porosity in the aluminum alloy automotive wheel during low-pressure die casting. Int. Metalcast **10**, 32–42 (2016). https://doi.org/10.1007/s40962-015-0008-0
2. O. Özaydın, A.Y. Kaya, D. Dispinar, Effect of Li additions and holding time on the mechanical properties of the AlSi9Mg alloys. Metall. Italiana **0026–0843**(113), 19–24 (2021)
3. I.A. Essienubong, O. Ikechukwu, P.O. Ebunilo, Comparison of aluminium wheel to steel wheel in relation to weight and fuel consumption (energy) in automobiles. Indust. Syst. Eng. **1**(1), 1–9 (2016). https://doi.org/10.22399/ijcesen.913166
4. E. Erzi, M. Tiryakioğlu, A simple procedure to determine incoming quality of aluminum alloy ingots and its application to A356 Alloy Ingots. Int. Metalcast **14**, 999–1004 (2020). https://doi.org/10.1007/s40962-020-00414-5
5. M.A. Elahi, S.G. Shabestari, Effect of various melt and heat treatment conditions on impact toughness of A356 aluminum alloy. Transact. Nonferrous Metals Soc. China **26**(4), 956–965 (2016). https://doi.org/10.1016/s1003-6326(16)64191-2
6. G.K. Sigworth, The modification of Al-Si casting alloys: important practical and theoretical aspects. Int. Metalcast **2**, 19–40 (2008). https://doi.org/10.1007/BF03355425
7. S. Shivkumar, C. Keller, M. Trazzera, D. Apelian, Precipitation hardening in A356 alloys, in *Production, refining fabrication and recycling of light metals*. (Elsevier, Netharland, 1990), pp. 264–278
8. F. Paray, B. Kulunk, J.E. Gruzleski, Impact properties of Al-Si foundry alloys. Int. J. Cast Metals Res. **13**(1), 17–37 (2000). https://doi.org/10.1080/13640461.2000.11819385
9. C. Do Lee, Variability in the impact properties of A356 aluminum alloy on microporosity variation. Mater. Sci. Eng.: A. **565**, 187–195 (2013). https://doi.org/10.1016/j.msea.2012.12.029
10. N.D. Alexopoulos, A. Stylianos, Impact mechanical behaviour of Al–7Si–Mg (A357) cast aluminum alloy the effect of artificial aging. Mater.s Sci. Eng. A **528**(19–20), 6303–6312 (2011). https://doi.org/10.1016/j.msea.2011.04.086
11. S. Shivkumar, L. Wang, C. Keller, Impact properties of A356–T6 alloys. J. Mater. Eng. Perform. **3**(1), 83–90 (1994). https://doi.org/10.1007/bf0265450
12. Z. Ma, A.M. Samuel, H.W. Doty, S. Valtierra, F.H. Samuel, Effect of Fe content on the fracture behaviour of Al–Si–Cu cast alloys. Mater. Des. **57**, 366–373 (2014). https://doi.org/10.1016/j.matdes.2014.01.037
13. S. Murali, K.S. Raman, K.S.S. Murthy, Effect of magnesium, iron (impurity) and solidification rates on the fracture toughness of Al 7Si 03 Mg casting alloy.

Mater. Sci. Eng. A **151**(1), 1–10 (1992). https://doi.org/10.1016/0921-5093(92)90175-Z
14. C.H. Caceres, C.J. Davidson, J.R. Griffiths, Q.G. Wang, The effect of Mg on the microstructure and mechanical behavior of Al-Si-Mg casting alloys. Metall. and Mater. Trans. A. **30**(10), 2611–2618 (1999). https://doi.org/10.1007/s11661-999-0301-8
15. Y.G. Kim, H. Fujii, T. Tsumura, T. Komazaki, K. Nakata, Fracture behaviour of grain refined A356 cast aluminium alloy: tensile and Charpy impact specimens. Mater. Sci. Eng. A **415**(1), 250–254 (2006)
16. Q.G. Wang, C.H. Cáceres, The fracture mode in Al–Si–Mg casting alloys. Mater. Sci. Eng., A **241**(1–2), 72–82 (1998). https://doi.org/10.1016/S0921-5093(97)00476-0
17. A.M. Samuel, H.W. Doty, S. Valtierra, F.H. Samuel, Effect of grain refining and Sr-modification interactions on the impact toughness of Al–Si–Mg cast alloys. Mater. Des. **1980–2015**(56), 264–273 (2014). https://doi.org/10.1016/j.matdes.2013.10.029
18. E. Tillová, M. Chalupová, K. Borko, L. Kuchariková, Changes of fracture surface in recycled A356 cast alloy. Mater. Today: Proc. **3**(4), 1183–1188 (2016). https://doi.org/10.1016/j.matpr.2016.03.009
19. M. Merlin, G. Timelli, F. Bonollo, G.L. Garagnani, Impact behaviour of A356 alloy for low-pressure die casting automotive wheels. J. Mater. Process. Technol. **209**(2), 1060–1073 (2009). https://doi.org/10.1016/j.jmatprotec.2008.03.027
20. M. Lalpoor, D. G. Eskin, L. Katgerman, (2008) Investigation of fracture behavior of high strength aluminum alloys in the as-cast condition. In: Proceedings of the 11th International Conference on Aluminium Alloys, 22-26 September 2008, Aachen, Germany. Wiley: New Jersey
21. W. D., Callister, D. G. Rethwisch, *Materials science and engineering: an introduction*, vol. 9 (Wiley, New York, 2018)
22. T.M. Osman, J. D. Rigney, (2000) Introduction to the mechanical behavior of metals, mechanical testing and evaluation. In: ASM Handbook. Vol. 8 p 35
23. E. Aguirre-De la Torre, U. Afeltra, C.D. Gómez-Esparza, J. Camarillo-Cisneros, R. Pérez-Bustamante, R. Martínez-Sánchez, Grain refiner effect on the microstructure and mechanical properties of the A356 automotive wheels. J. Mater. Eng. Perform. **23**, 581–587 (2014). https://doi.org/10.1007/s11665-013-0596-x
24. P. Li, M.D. Maijer, T.C. Lindley, P.D. Lee, Simulating the residual stress in an A356 automotive wheel and its impact on fatigue life. Metall. Mater. Trans. B **38**, 505–515 (2007). https://doi.org/10.1007/s11663-007-9050-5
25. A.M. Samuel, H.W. Doty, S. Valtierra, F.H. Samuel, On the impact properties and fracture mechanisms of A356.2 type cast alloys. Int. Metalcast **11**, 766–777 (2017). https://doi.org/10.1007/s40962-016-0122-7
26. K.A. Abuhasel, M.F. Ibrahim, E.M. Elgallad, F.H. Samuel, On the impact toughness of Al–Si cast alloys. Mater. Des. **91**, 388–397 (2016). https://doi.org/10.1016/j.matdes.2015.11.072
27. Z. Ma, A.M. Samuel, F.H. Samuel, H.W. Doty, Effect of Fe content and cooling rate on the impact toughness of cast 319 and 356 aluminum alloys. AFS Trans. **111**, 255–265 (2003)
28. X.J. Yua, Y.L. Lub, F.X. Zhuc, X.C. Lid, Effect of heat treatment on microstructures and mechanical properties of A356 alloy by low pressure casting. Adv. Mater. Res. ISSN **1662–8985**(1096), 319–324 (2015). https://doi.org/10.4028/www.scientific.net/amr.1096.319
29. R. K. Nanstad, R. L. Swain, R. G. Berggren, Influence of thermal conditioning media on Charpy specimen test temperature. In Charpy Impact Test: Factors and Variables. ASTM International, (1990)
30. E. Fiorese, F. Bonollo, G. Timelli, L. Arnberg, E. Gariboldi, New classification of defects and imperfections for aluminum alloy castings. Int. Metalcast **9**, 55–66 (2015). https://doi.org/10.1007/BF03355602
31. M. Djurdjevic, H. Jiang, J. Sokolowski, On-line prediction of aluminum-silicon eutectic modification level using thermal analysis /. Mater. Charact. **46**, 31–38 (2001). https://doi.org/10.1016/s1044-5803(00)00090-5
32. N. Tenekedjiev, H. Mulazimoglu, B. Closset, J. Gruzleski, *Microstructures and thermal analysis of strontium-treated aluminum - silicon alloys* (American Foundrymen's Society Des Plaines, IL, USA, 1995)
33. M. Warmuzek, 2004. Aluminium–Silicon Casting Alloys: Atlas of Microfractographs, 1st ed. ASM International, (2004)